Food Science of Animal Products

Research Article

Electrochemical sensor based on Pd@Nb_2C nanocomposites for rapid and sensitive detection of ciprofloxacin

Haohao Zhang[1,§], Yujiao Sun[1,§], Hailing Luo[2], Nan Cheng[1] ✉, Hao Zhang[1] ✉

[1] *College of Food Science and Nutritional Engineering, China Agricultural University, Beijing 100083, China*
[2] *State Key Laboratory of Animal Nutrition, College of Animal Science and Technology, China Agricultural University, Beijing 100193, China*
§ These authors contributed equally to this article.
✉Address correspondence to Nan Cheng, Goodluckchengnan@163.com; Hao Zhang, zhanghaocau@cau.edu.cn
Received: September 22, 2024; Revised: October 21, 2024; Accepted: October 31, 2024

Abstract: This study introduced an electrochemical sensor for the rapid, sensitive, and accurate detection of ciprofloxacin (CIP). The sensor utilized a screen-printed carbon electrode (SPCE) modified with Pd@Nb_2C nanocomposites, which were prepared through the *in-situ* reduction of palladium nitrate on Nb_2C nanosheets, resulting in a uniform distribution of Pd nanoparticles. Subsequently, they were drop-coated onto the SPCE surface, forming a Pd@Nb_2C/SPCE electrochemical sensing platform. The electrochemical analysis demonstrated the excellent electrochemical performance of the sensor. Pd@Nb_2C/SPCE showed a consistent linear correlation between redox peak current (I_P) and CIP concentration (c_{CIP}) in the range of 10–150 μmol/L, boasting a detection limit of 3 μmol/L. Notably, this technique tracked CIP in both whole and skimmed milk, achieving a high recoveries of 96.36%–105.40% (n = 3). Moreover, the sensor exhibited exceptional selectivity towards CIP, remaining unaffected by various interferences such as sulphonamide, amoxicillin, tetracycline, and chloramphenicol. These findings hold enormous promise for enabling real-time and rapid monitoring of CIP in milk.

Keywords: ciprofloxacin; electrochemical sensor; nanocomposites

Citation: H. H. Zhang, Y. J. Sun, H. L. Luo, et al., Electrochemical sensor based on Pd@Nb_2C nanocomposites for rapid and sensitive detection of ciprofloxacin, Food Sci. Anim. Prod. 3 (2025) 9240097. https://doi.org/10.26599/FSAP.2025.9240097.

1 Introduction

The milk, globally renowned for its rich nutritional content including protein, carbohydrates, fats, and vitamins, plays a pivotal role in promoting human health across all age groups[1–2]. Ciprofloxacin (CIP), a potent quinolone antibiotic, demonstrates significant antibacterial activity against both Gram-positive and Gram-negative bacteria[3]. In animal husbandry, administered through intravenous injection or added to feed, it finds widespread applications in the prevention and treatment of diseases among dairy cows[4]. However, the improper use of CIP by unethical dairy farmers has led to the presence of CIP residues in milk, which poses various health risks to humans, such as poisoning and allergic reactions[5–6]. To safeguard human life and health, numerous countries have established maximum residue limit (MRL) for CIP in animal-derived foods[7]. Consequently, it is crucial to develop accurate assays for CIP detection. Current detection methods for CIP include high performance liquid chromatography[8], capillary electrophoresis[9], and liquid chromatography-mass spectrometry[10]. While these methods offer sensitivity in detection, they have limitations such as the requirement for specialized and costly equipment, as well as complex sample pre-treatment processes[11–12]. These challenges impede the attainment of real-time and rapid detection of CIP. Electrochemical methods offer numerous advantages over traditional detection techniques for detecting and quantifying CIP. These benefits encompass simplicity, rapidity, excellent selectivity, high sensitivity, and cost-effectiveness[13]. However, it is crucial to acknowledge that electrochemical detection using traditional electrodes may face interference from biological factors and lead to poor detection stability due to electrode passivation[14–16]. In the domain of electrochemical analysis, the adoption of nanomaterial-modified electrodes for electrochemical sensing has gained significant attention in recent years[17–19]. Fotouhi et al.[20] synthesized multi-walled carbon nanotubes (MWCNT) and modified a glassy carbon electrode (GCE) with them to develop an electrochemical sensor for detecting CIP. This method demonstrated validated accuracy and operability, with a detection limit of 6.0 μmol/L. Particularly, MXenes, a class of nanomaterials comprising transition metal carbide and/or nitride nanomaterials, have captivated significant interest within the scientific community by their unique structure and wide-ranging physical and chemical properties[21–22]. MXenes possess a layered structure, exceptional conductivity, and environmentally friendly characteristics[23], rendering them versatile across various domains including energy storage, environmental remediation, biomedicine, and electrochemical sensing, among others[24–26]. The primary source of MXenes originates from the ternary precursor material MAX phase, which is obtained by selectively etching the A layer. Here, M represents the early transition metal, A denotes the elements in the 13th or 14th group, and X signifies C and/or N. The standardized formula for the chemical composition of MXenes is $M_{n+1}X_nT_x$ (n = 1–4), where T_x represents surface-terminating functional groups (such as hydroxyl, fluorine, oxygen, and chlorine), formed during the etching process[27]. Currently, theoretically, over 200

potential methods for producing MXenes have been anticipated[28]. In recent years, there has been a significant surge in academic research focusing on Nb_2C, a substantial subgroup within the MXenes family. The intriguing physicochemical properties and distinct magnetic characteristics of this metal carbide offer abundant opportunities for investigation[29]. Surface modification has emerged as a successful approach to stabilize MXenes, as their standalone utilization for electrochemical sensing often lacks stability[30–31]. To improve the electrochemical properties of Nb_2C, Arif et al.[32] synthesized a Nb_2C/ZnS nanocomposite, then applied this composite onto a GCE for the electrochemical detection of dopamine. The resulting electrochemical sensor exhibited a low detection limit, high sensitivity, and excellent selectivity toward dopamine. The stabilized Pd/MXene complexes have also been used for highly sensitive electrochemical detection[33–34]. In this study, an electrochemical sensor for detecting CIP (Figure 1) was developed using Pd@Nb_2C nanocomposites. The synthesis of Pd@Nb_2C involved three steps: hydrofluoric acid etching, tetrapropylammonium hydroxide (TPAOH) intercalation, and palladium nitrate self-reduction. The resulting material was drop-cast onto screen-printed carbon electrode (SPCE) to create a Pd@Nb_2C/SPCE electrochemical sensor[14,27]. CIP underwent oxidation on the SPCE surface, leading to an increase in its redox peak current (I_P). Square wave voltammetry (SWV) was used to detect CIP, confirming a linear relationship between I_P and the CIP concentration (c_{CIP}).

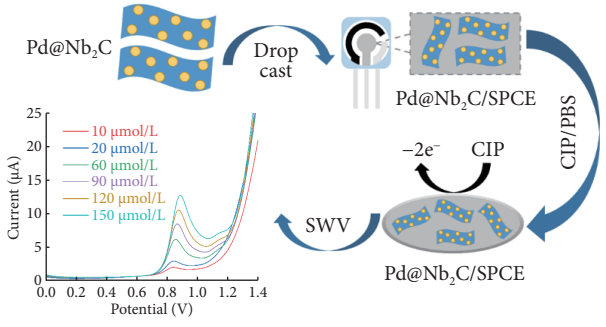

Figure 1 Fabrication technology of Pd@Nb_2C/SPCE sensing platform and its application in CIP detection. PBS, phosphate buffer solution.

2 Materials and methods

2.1 Materials

Nb_2AlC was obtained from Jiangsu XFNANO Materials Tech Co., Ltd. (Nanjing, China). CIP, lactose (LAC), and hydrofluoric acid (HF) aqueous solution (40%) were supplied by Shanghai Macklin Biochemical Co., Ltd. (Shanghai, China). Potassium hexacyanoferrate (II) trihydrate, disodium hydrogen phosphate dodecahydrate, and sodium phosphate monobasic dehydrate were procured from Tianjin Yongda Chemical Reagent Co., Ltd. (Tianjin, China). The analytically pure KCl, NaCl and $CaCl_2$ were supplied by Sinopharm Chemical Reagent Co., Ltd. (Shanghai, China). Potassium ferricyanide, palladium nitrate dehydrate ($Pd(NO_3)_2{\cdot}2H_2O$), sulfanilamide (SUL), chloramphenicol (CHL), amoxicillin crystalline (AMO), tetracycline (TET), and TPAOH aqueous solution (25%) were purchased from Shanghai Yien Chemical Technology Co., Ltd. (Shanghai, China). Milk samples were commercially available Yili whole and skimmed milk. All chemical reagents and pharmaceuticals were used as received and did not have to be purified again. Deionised (DI) water was used during the whole experiment.

2.2 Apparatus

Scanning electron microscope (SEM) images were obtained using a Zeiss Gemini SEM 300 field emission SEM (Jena, Germany). Transmission electron microscope (TEM) images were captured using a Hitachi HT7700 TEM (Tokyo, Japan). Fourier transform infrared (FTIR) spectra were obtained using a PerkinElmer FTIR spectrometer (Akron, Ohio, USA). X-ray diffraction (XRD) analyses of powder samples were performed using a Rigaku Ultima IV diffractometers (Tokyo, Japan) equipped with graphitized monochromatic Cu Kα radiation. X-ray photoelectron spectroscopy (XPS) procedures were performed on the Thermo Scientific Kα X-ray photoelectron spectrometer (Waltham, MA, USA). Cyclic voltammetry (CV) and SWV electrochemical spectra were acquired at the CHI-1080C electrochemical workstation (Shanghai, China). Electrochemical impedance spectra (EIS) were measured by the CHI-760E electrochemical workstation (Shanghai, China). All electrochemical experiments were accomplished using modified SPCE based on a three-electrode system.

2.3 Preparation of Pd@Nb_2C nanocomposites

Nb_2AlC powder (2.5 g) was immersed in 15 mL of 40% HF aqueous solution and allowed to react at the appropriate temperature for 48 h. After the etching process, the sample was washed multiple times in DI water, centrifuged at 4 000 r/min until the pH reached approximately 5.5, and then filtered to obtain the multilayered Nb_2C. The collected powder was dispersed in 15 mL of 25% TPAOH solution and agitated vigorously at 25 ℃ for 72 h. Afterward, the sample was washed in DI water and centrifuged three times at 12 000 r/min. The powder was then dissolved in DI water and centrifuged at 3 500 r/min to obtain the Nb_2C colloid. The Nb_2C nanosheets were obtained through lyophilization. Initially, Nb_2C powder (15 mg) was homogeneously mixed with 30 mL of DI water and sonicated for 10 min. Subsequently, 1 mg/mL $Pd(NO_3)_2{\cdot}2H_2O$ solution was added to the Nb_2C dispersion to achieve an overall starting loading of 20% (*m*/*m*) of Pd onto Nb_2C. The mixture was sonicated for 20 min followed by constant agitation at room temperature for 24 h. After the reaction, the mixture was washed in DI water, and centrifuged three times at 12 000 r/min, followed by freeze-drying to produce Pd@Nb_2C nanocomposites.

2.4 Preparation of Pd@Nb_2C/SPCE

Pd@Nb_2C was uniformly dispersed in anhydrous ethanol in the appropriate quantity. A 4 μL portion of the mixture was then drop-cast onto the SPCE surface and left to cure in the air to create the electrochemical sensing platform based on Pd@Nb_2C/SPCE.

2.5 Electrochemical experiments

A series of electrochemical experiments, including CV, EIS, and SWV were conducted using Pd@Nb_2C/SPCE, Nb_2C/SPCE, and bare SPCE concurrently. For CV and EIS measurements, both bare SPCE and modified SPCE were transferred into 5 mmol/L $[Fe(CN)_6]^{3-/4-}$ within 0.1 mol/L KCl. SWV was employed to explore

the optimal pH for electrochemical sensing of CIP by the Pd@Nb_2C/SPCE sensor in the presence of 0.1 mmol/L CIP in PBS at various pH levels. SWV profiles were recorded under the optimal conditions in PBS containing different concentrations of CIP using the Pd@Nb_2C/SPCE electrochemical sensing platform. A linear curve was then plotted between I_P and c_{CIP}. The selectivity of Pd@Nb_2C/SPCE for CIP needed to be assessed due to the complex composition of milk and the possible presence of other contaminating residues. The SWV profile of 0.1 mmol/L CIP was determined using the Pd@Nb_2C/SPCE sensor under optimal detection conditions, the interferences of Na^+, Ca^{2+}, LAC, SUL, CHL, TET, and AMO at a concentration of 10 μmol/L in CIP detection were investigated. Furthermore, the stability of the electrochemical sensors was evaluated by measuring the CV signals several times consecutively in $[Fe(CN)_6]^{3-/4-}$ buffer and the SWV signals several times consecutively in PBS containing 0.1 mmol/L CIP (at optimal pH).

2.6 Real sample preparation

The practical utility of Pd@Nb_2C/SPCE electrochemical sensors was evaluated for detecting CIP in actual milk samples. Initially, proteins in the milk samples were eliminated using anhydrous ethanol, followed by the removal of excess ethanol via rotary evaporation. The treated milk was then diluted tenfold with PBS, and various concentrations (10, 50, 100 μmol/L) of CIP were introduced for analysis.

2.7 Statistical analysis

The ZView software (Scribner Associates Inc., USA) was used to fit the equivalent characteristic parameters of impedance. The Origin 2023b (Origin Lab Co., Northampton, MA, USA) was used to analyze the data and draw the line chart. Each indicator measurement was repeated three times, and the value was expressed as mean ± standard deviation.

3 Results and discussion

3.1 Micro-morphological characterization of nanocomposites

The synthesized nanomaterials were characterized to determine their microscopic morphology using SEM and TEM. Nb_2C was obtained by immersing the precursor Nb_2AlC in HF, leveraging the remarkably high stability of the Nb–C bond[35]. SEM images of Nb_2AlC before and after HF etching are presented in Figures 2A and B. The presence of a lamellar structure characteristic of MXenes is visible in Figure 2B, indicating the successful and selective removal of the Al layer from the MAX phase by HF. Under vigorous stirring, continuous ion exchange between protons (H^+) and tetrapropylammonium ions (TPA^+) facilitated the expansion and delamination of the multilayered Nb_2C[36]. Figure 2C displays the exfoliated nanosheets with transparent features, confirming their ultrathin characteristics. Nb_2C nanosheets served as both substrate and reducing agent, enabling the self-reduction of $Pd(NO_3)_2$ and Pd nanoparticle deposition on the surface of the material, forming Pd@Nb_2C[37]. As illustrated in Figure 2D, well-dispersed spherical-like Pd nanoparticles were present on the surface of the Nb_2C nanosheets, attributed to the reduction of metal ions by the active groups on Nb_2C.

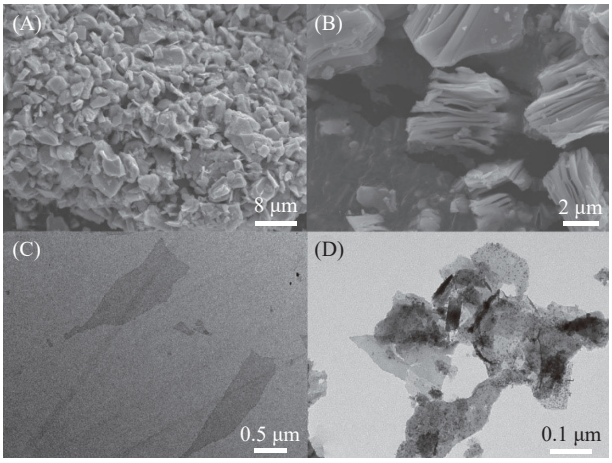

Figure 2 SEM images of (A) Nb_2AlC and (B) multilayered Nb_2C, TEM images of (C) Nb_2C nanosheets and (D) Pd@Nb_2C.

3.2 Spectral characterization of nanocomposites

Figure 3A presents the FTIR spectra corresponding to the three materials. Initially, the bands in the Nb_2AlC spectrum were limited, but they became more prominent after etching, indicating the emergence of surface-terminating functional groups during this process[38]. The bands at 593 and 1 616 cm^{-1} were attributed to the Nb–C and C=C structures in Nb_2C, respectively[39]. Additionally, bands associated with the etching process included the C–H band at 2 972 cm^{-1}, the C=O band at 1 724 cm^{-1}, and the C–F band at 1 083 cm^{-1}. The band at 1 622 cm^{-1} in the spectrum of Pd@Nb_2C resulted from the combined effect of C=O and Pd nanoparticles[40].

Figure 3B displays the XRD spectra of Nb_2AlC, Nb_2C, and Pd@Nb_2C. The XRD diffractogram of Nb_2AlC matched the previously reported profile (JCPDF No. 030-0033)[41]. After etching, the characteristic peak at 2θ 38.9° corresponding to Al was nearly completely eliminated. Moreover, the intensity of the (002) peak at 2θ 12.76° was diminished and shifted to a lower angle of 7.14° due to a significant increase in the C lattice parameter. This change indicated an expansion of the layer spacing and a separation of the lamellae[42]. In the XRD spectrum of Pd@Nb_2C, the characteristic peaks for (111), (200), and (220) at 2θ 40.14°, 46.22°, and 67.88°, respectively, corresponded to Pd nanoparticles on the surface of Nb_2C nanosheets[43]. The position of the (002) peak remained unchanged suggesting no influence of Pd nanoparticles on the structural properties of the nanosheets.

To further investigate the characteristics of the material, XPS spectroscopy was conducted (Figure 3C). The results indicated that etching significantly amplified the signal intensity of the Nb element while nearly eliminating the signal of the Al element[44]. Furthermore, the presence of the characteristic peak of Pd 3d, absent in Nb_2C, in the XPS spectrum of Pd@Nb_2C suggested that the Pd nanoparticles were effectively attached to the few-layer Nb_2C nanosheets. The XPS spectrum of Nb 3d is shown in Figure 3D. The bands observed at binding energies of 214.63 and 211.98 eV were identified as Nb $3d_{3/2}$ and Nb $3d_{5/2}$ orbitals, respectively. The distinct valence states of Nb were attributed to oxidation during the etching process, while the remaining bands were attributed to Nb binding with surface functional groups[45].

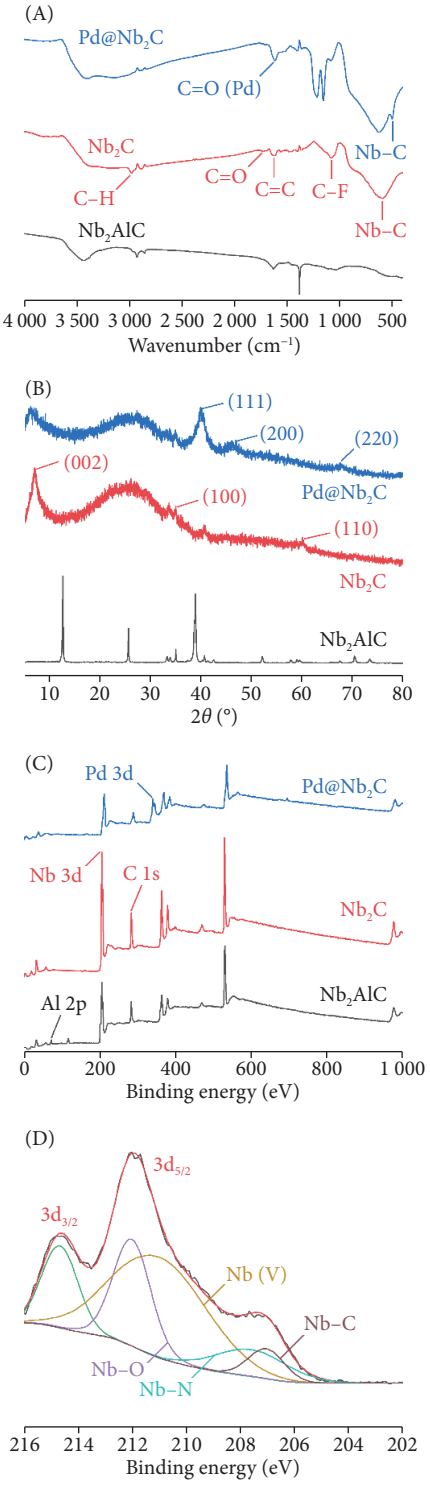

Figure 3 (A) FTIR spectra, (B) XRD patterns, and (C) full-scan XPS spectra of Nb_2AlC, Nb_2C, and Pd@Nb_2C. (D) High resolution XPS spectrum of Nb 3d.

3.3 Electrochemical performances of Pd@Nb_2C/SPCE

The efficacy of the nanocomposite electrodes was evaluated through the measurement of the EIS and CV curves. The electrodes exhibited distinctive redox peaks, as illustrated in Figure 4A. Notably, the peak current intensity of Pd@Nb_2C/SPCE surpassed that of Nb_2C/SPCE and SPCE. This observation suggested the synergistic effect between the Pd nanoparticles and Nb_2C nanosheets in enhancing the electrical conductivity of Nb_2C. Pd nanoparticles are known to improve the rate of charge transfer and the sensitivity of electrochemical detection. Furthermore, Pd@Nb_2C/SPCE exhibited the highest oxidation peak current in the CV detection of CIP (Figure S1). During this process, the H atom on the CIP piperazine ring attached to N underwent oxidation to form a hydroxyl group[46], leading to electron transfer and the generation of an oxidation characteristic peak. In addition, the presence of asymmetric peaks showed the reversibility of the CIP oxidation process.

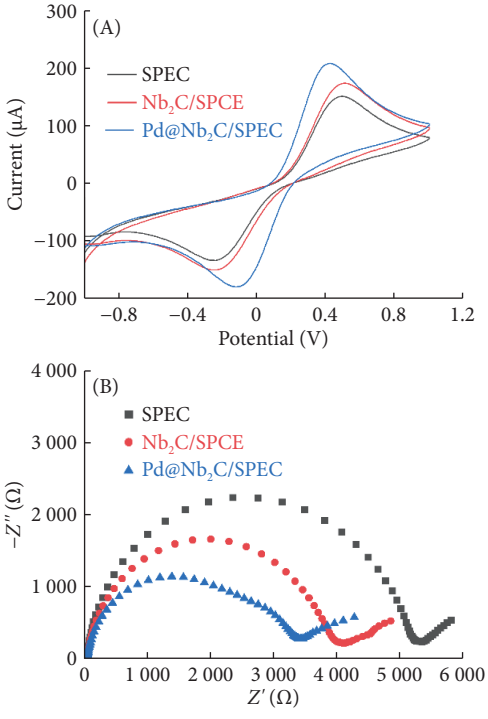

Figure 4 (A) Cyclic voltammograms and (B) Nyquist plots of various modified electrodes in 0.1 mol/L KCl with 5 mmol/L $[Fe(CN)_6]^{3-/4-}$.

The Nyquist plots for Pd@Nb_2C/SPCE, Nb_2C/SPCE, and SPCE are shown in Figure 4B. The charge-transfer resistance (R_{ct}) is indicated by the diameter of the Nyquist semicircle, where a larger diameter reflects a higher resistance to charge transfer[47]. Notably, Pd@Nb_2C/SPCE had the smallest diameter, suggesting the highest conductivity and the smallest resistivity. The results were consistent with the CV detection data, reinforcing the superior electrochemical performance of the nanocomposite electrodes.

3.4 Electrochemical sensing of CIP

The optimal pH for CIP electrochemical detection was determined to be 7.0 (Figure S2). Using the Pd@Nb_2C/SPCE electrochemical sensor, the SWV curves of various CIP concentrations were obtained at this pH. In Figure 5A, the intensity of I_P increased as c_{CIP} was progressively raised from 10 to 150 μmol/L. Additionally, an analytical curve was constructed between I_P and c_{CIP} (Figure 5B). The curve displayed a strong linear relationship (I_P = 0.062 9c_{CIP} + 0.344 1 (R^2 = 0.996 0)). With a signal-to-noise ratio (R_{SN}) of 3, the limit of detection (LOD) was estimated to be approximately 3 μmol/L, indicating that the high sensitivity of the Pd@Nb_2C/SPCE for the detection of CIP.

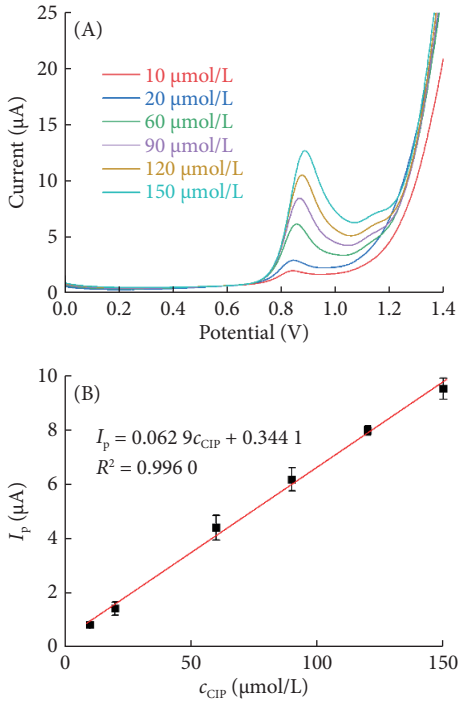

Figure 5 (A) SWV curves of the Pd@Nb_2C/SPCE electrochemical sensing platform with different concentrations of CIP and (B) linear relationship between I_P and c_{CIP} from 10 to 150 μmol/L.

3.5 Selectivity and stability of Pd@Nb_2C/SPCE platform

The current response for CIP changed by approximately 5% for each interferent (Figure 6). When all interferents and CIP (0.1 mmol/L) were mixed, the electrical signal response closely resembled that of CIP alone. These results suggested strong selectivity of the constructed sensor for CIP.

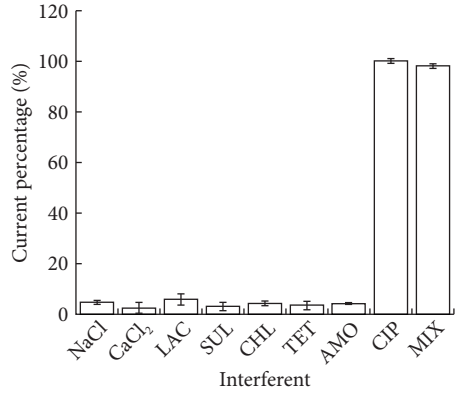

Figure 6 Interference studies of CIP in the presence of different substances with concentration levels of 0.1 mmol/L for CIP and 10 μmol/L for the interferents.

To assess the stability of the sensor, 15 consecutive measurements of 5 mmol/L $[Fe(CN)_6]^{3-/4-}$ were performed using the CV method, and 15 consecutive measurements of 0.1 mmol/L CIP were performed using the SWV method. Throughout this series, both the CV and SWV signals remained steady (Figure S3), suggesting excellent consistency in the detection process facilitated by Pd@Nb_2C/SPCE.

3.6 Determination performance of Pd@Nb_2C/SPCE in real samples

Pd@Nb_2C/SPCE was employed to assess the utility of this electrochemical sensor in detecting CIP in real milk samples, including whole and skimmed milk. Using the linear curve between I_P and c_{CIP}, different concentrations of CIP (10, 50, and 100 μmol/L) were added to the samples to evaluate the level of CIP in the spiked milk samples. As presented in Table 1, the measured and spiked c_{CIP} values exhibited a high degree of similarity, with good recoveries (96.36%–105.40%) and low relative standard deviations (0.83%–3.59%) (n = 3). The results underscoreed the capability of Pd@Nb_2C/SPCE in monitoring CIP in milk with high utility.

Table 1 Determination results of CIP in milk samples using Pd@Nb_2C (n = 3).

Sample	Spiked level (μmol/L)	Detected value (μmol/L)	Average spiked recovery (%)	Relative standard deviation (%)
Whole milk	10	9.68 ± 0.14	96.84	1.45
	50	52.70 ± 0.44	105.40	0.83
	100	96.36 ± 1.41	96.36	1.46
Skimmed milk	10	10.42 ± 0.14	104.18	1.34
	50	50.51 ± 1.81	101.03	3.59
	100	98.37 ± 1.29	98.37	1.31

Note: Detected value is expressed as mean ± standard deviation.

The developed electrochemical sensing platform for CIP detection, utilizing Pd@Nb_2C/SPCE, was benchmarked against previous studies reported in the literature on electrochemical approaches for CIP monitoring (Table S1). This study demonstrated sensitivity with a limit of detection comparable to other electrochemical sensors documented in existing literature. Moreover, the linear range of the approach was broad. It is important to highlight that the low manufacturing cost of Pd@Nb_2C nanocomposites, along with their ease of electrode modification and excellent selectivity for target monitoring, rendering them promising options for application in real-world samples.

4 Conclusion

In this study, a novel Pd@Nb_2C nanocomposite electrode serving as an electrochemical sensing platform for rapid and accurate CIP monitoring in both whole and skimmed milk was developed. The technique offered a detection limit of 3 μmol/L and a wide linear range (10–150 μmol/L). Additionally, the Pd@Nb_2C/SPCE demonstrated resilience against potential interfering substances and exhibited exceptional selectivity for CIP. High recoveries and low relative standard deviations underscored the reliability of the sensor in detecting CIP residues in milk.

Conflicts of interest

The authors declare no conflict of interest.

Acknowledgments

This work was supported by the Program of Chinese National Mutton Sheep Industrial Technology System (CARS-38) and the 111 Project from the Education Ministry of China (B18053).

Appendix A. Supplementary data

Supplementary data associated with this article can be found in the online version, at https://doi.org/10.26599/FSAP.2025.9240097.

References

[1] I. C. Antunes, R. Bexiga, C. Pinto, et al., Cow's milk in human nutrition and the emergence of plant-based milk alternatives, Foods 12 (2023) 99. https://doi.org/10.3390/foods12010099.

[2] F. H. You, Z. R. Wen, R. S. Yuan, et al., Selective and ultrasensitive detection of ciprofloxacin in milk using a photoelectrochemical aptasensor based on $Ti_3C_2/Bi_4VO_8Br/TiO_2$ nanocomposite, J. Electroanal. Chem. 914 (2022) 116285. https://doi.org/10.1016/j.jelechem.2022.116285.

[3] S. V. Kergaravat, A. Maria Gagneten, S. R. Hernandez, Development of an electrochemical method for the detection of quinolones: application to cladoceran ecotoxicity studies, Microchem. J. 141 (2018) 279–286. https://doi.org/10.1016/j.microc.2018.05.039.

[4] M. Majdinasab, K. Mitsubayashi, J. L. Marty, Optical and electrochemical sensors and biosensors for the detection of quinolones, Trends Biotechnol. 37 (2019) 898–915. https://doi.org/10.1016/j.tibtech.2019.01.004.

[5] N. R. Jalal, T. Madrakian, A. Afkhami, et al., Polyethylenimine@Fe_3O_4@carbon nanotubes nanocomposite as a modifier in glassy carbon electrode for sensitive determination of ciprofloxacin in biological samples, J. Electroanal. Chem. 833 (2019) 281–289. https://doi.org/10.1016/j.jelechem.2018.12.004.

[6] D. Liang, Y. J. Xu, F. Peng, et al., Plasmonic metal NP-bismuth composite film with amplified SERS activity for multiple detection of pesticides and veterinary drugs, Chem. Eng. J. 474 (2023) 145933. https://doi.org/10.1016/j.cej.2023.145933.

[7] D. G. Pinacho, F. Sanchez-Baeza, M. I. Pividori, et al., Electrochemical detection of fluoroquinolone antibiotics in milk using a magneto immunosensor, Sensors 14 (2014) 15965–15980. https://doi.org/10.3390/s140915965.

[8] T. Gezahegn, B. Tegegne, F. Zewge, et al., Salting-out assisted liquid-liquid extraction for the determination of ciprofloxacin residues in water samples by high performance liquid chromatography-diode array detector, BMC Chem. 13 (2019) 28. https://doi.org/10.1186/s13065-019-0543-5.

[9] R. Colombo, A. Papetti, Advances in the analysis of veterinary drug residues in food matrices by capillary electrophoresis techniques, Molecules 24 (2019) 4617. https://doi.org/10.3390/molecules24244617.

[10] A. Parpounas, V. Litskas, E. Hapeshi, et al., Assessing the presence of enrofloxacin and ciprofloxacin in piggery wastewater and their adsorption behaviour onto solid materials, with a newly developed chromatographic method, Environ. Sci. Pollut. Res. 24 (2017) 23371–23381. https://doi.org/10.1007/s11356-017-9849-9.

[11] J. Li, K. Chen, Y. Su, et al., Paper-based biosensors based on multiple recognition modes for visual detection of microbially contaminated food, J. Future Foods 4 (2024) 61–70. https://doi.org/10.1016/j.jfutfo.2023.05.007.

[12] Y. W. Wang, B. Zhang, M. J. Guo, et al., Rapid detection of cordycepin in food by surface enhanced Raman technque, J. Future Foods 3 (2023) 24–28. https://doi.org/10.1016/j.jfutfo.2022.09.004.

[13] H. Karimi-Maleh, F. Karimi, M. Alizadeh, et al., Electrochemical sensors, a bright future in the fabrication of portable kits in analytical systems, Chem. Rec. 20 (2020) 682–692. https://doi.org/10.1002/tcr.201900092.

[14] P. A. Rasheed, R. P. Pandey, K. A. Jabbar, et al., Sensitive electrochemical detection of *L*-cysteine based on a highly stable Pd@$Ti_3C_2T_x$ (MXene) nanocomposite modified glassy carbon electrode, Anal. Methods 11 (2019) 3851–3856. https://doi.org/10.1039/c9ay00912d.

[15] P. H. Deng, C. Q. Zhou, H. Sun, et al., Manganese cobalt sulfide nanoparticles wrapped by reduced graphene oxide: a fascinating nanocomposite as an efficient electrochemical sensing platform for vanillin determination, J. Future Foods 5 (2025) 162–171. https://doi.org/10.1016/j.jfutfo.2024.05.005.

[16] Y. Zhao, Y. J. Xu, X. H. Jing, et al., SERS-active plasmonic metal NP-$CsPbX_3$ films for multiple veterinary drug residues detection, Food Chem. 412 (2023) 135420. https://doi.org/10.1016/j.foodchem.2023.135420.

[17] Y. J. Sun, X. Wang, H. Zhang, Sensitive and stable electrochemical sensor for folic acid determination using a ZIF-67/AgNWs nanocomposite, Biosensors 12 (2022) 382. https://doi.org/10.3390/bios12060382.

[18] Y. Zhao, J. J. Shao, Z. Jin, et al., Plasmon-enhanced electroreduction activity of Au-AgPd Janus nanoparticles for ochratoxin a detection, Food Chem. 412 (2023) 135526. https://doi.org/10.1016/j.foodchem.2023.135526.

[19] Y. C. Ouyang, B. J. Yeom, Y. Zhao, et al., Progress and prospects of chiral nanomaterials for biosensing platforms, Rare Metals 43 (2024) 2469–2497. https://doi.org/10.1007/s12598-023-02602-8.

[20] L. Fotouhi, M. Alahyari, Electrochemical behavior and analytical application of ciprofloxacin using a multi-walled nanotube composite film-glassy carbon electrode, Colloids Surf. B 81 (2010) 110–114. https://doi.org/10.1016/j.colsurfb.2010.06.030.

[21] P. Abdul Rasheed, R. P. Pandey, T. Gomez, et al., Nb-based MXenes for efficient electrochemical sensing of small biomolecules in the anodic potential, Electrochem. Commun. 119 (2020) 106811. https://doi.org/10.1016/j.elecom.2020.106811.

[22] C. Peng, P. Wei, X. Chen, et al., A hydrothermal etching route to synthesis of 2D MXene (Ti_3C_2, Nb_2C): enhanced exfoliation and improved adsorption performance, Ceram. Int. 44 (2018) 18886–18893. https://doi.org/10.1016/j.ceramint.2018.07.124.

[23] X. Z. Wu, P. Y. Ma, Y. Sun, et al., Application of MXene in electrochemical sensors: a review, Electroanalysis 33 (2021) 1827–1851. https://doi.org/10.1002/elan.202100192.

[24] X. T. Jiang, A. V. Kuklin, A. Baev, et al., Two-dimensional MXenes: from morphological to optical, electric, and magnetic properties and applications, Phys. Rep. 848 (2020) 1–58. https://doi.org/10.1016/j.physrep.2019.12.006.

[25] H. Lin, S. S. Gao, C. Dai, et al., A two-dimensional biodegradable niobium carbide (MXene) for photothermal tumor eradication in NIR-I and NIR-II biowindows, J. Am. Chem. Soc. 139 (2017) 16235–16247. https://doi.org/10.1021/jacs.7b07818.

[26] J. Li, X. Gao, L. Zhu, et al., Graphdiyne for crucial gas involved catalytic reactions in energy conversion applications, Energ. Environ. Sci. 13 (2020) 1326–1346. https://doi.org/10.1039/c9ee03558c.

[27] L. Gao, C. Ma, S. Wei, et al., Applications of few-layer Nb_2C MXene: narrow-band photodetectors and femtosecond mode-locked fiber lasers, ACS Nano 15 (2021) 954–965. https://doi.org/10.1021/acsnano.0c07608.

[28] Y. Gogotsi, B. Anasori, The rise of MXenes, ACS Nano 13 (2019) 8491–8494. https://doi.org/10.1021/acsnano.9b06394.

[29] Y. Xin, Y. X. Yu, Possibility of bare and functionalized niobium carbide MXenes for electrode materials of supercapacitors and field emitters, Mater. Des. 130 (2017) 512–520. https://doi.org/10.1016/j.matdes.2017.05.052.

[30] V. M. H. Ng, H. Huang, K. Zhou, et al., Recent progress in layered transition metal carbides and/or nitrides (MXenes) and their composites: synthesis and applications, J. Mater. Chem. A 5 (2017) 3039–3068. https://doi.org/10.1039/c6ta06772g.

[31] L. Li, N. Zhang, M. Y. Zhang, et al., Ag-nanoparticle-decorated 2D titanium carbide (MXene) with superior electrochemical

performance for supercapacitors, ACS Sustain. Chem. Eng. 6 (2018) 7442–7450. https://doi.org/10.1021/acssuschemeng.8b00047.

[32] N. Arif, S. Gul, M. Sohail, et al., Synthesis and characterization of layered Nb_2C MXene/ZnS nanocomposites for highly selective electrochemical sensing of dopamine, Ceram. Int. 47 (2021) 2388–2396. https://doi.org/10.1016/j.ceramint.2020.09.081.

[33] M. Rezayat, R. K. Blundell, J. E. Camp, et al., Green one-step synthesis of catalytically active palladium nanoparticles supported on cellulose nanocrystals, ACS Sustain. Chem. Eng. 2 (2014) 1241–1250. https://doi.org/10.1021/sc500079q.

[34] E. Satheeshkumar, T. Makaryan, A. Melikyan, et al., One-step solution processing of Ag, Au and Pd@MXene hybrids for SERS, Sci. Rep. 6 (2016) 32049. https://doi.org/10.1038/srep32049.

[35] J. B. Zhao, J. Wen, L. N. Bai, et al., One-step synthesis of few-layer niobium carbide MXene as a promising anode material for high-rate lithium ion batteries, Dalton Trans. 48 (2019) 14433–14439. https://doi.org/10.1039/c9dt03260f.

[36] O. Mashtalir, M. R. Lukatskaya, M. Q. Zhao, et al., Amine-assisted delamination of Nb_2C MXene for Li-ion energy storage devices, Adv. Mater. 27 (2015) 3501–3506. https://doi.org/10.1002/adma.201500604.

[37] R. P. Pandey, K. Rasool, V. E. Madhavan, et al., Ultrahigh-flux and fouling-resistant membranes based on layered silver/MXene ($Ti_3C_2T_x$) nanosheets, J. Mater. Chem. 6 (2018) 3522–3533. https://doi.org/10.1039/c7ta10888e.

[38] B. Anasori, Y. Xie, M. Beidaghi, et al., Two-dimensional, ordered, double transition metals carbides (MXenes), ACS Nano 9 (2015) 9507–9516. https://doi.org/10.1021/acsnano.5b03591.

[39] W. Acchar, J. R. B. da Silva, Surface characterization of alumina reinforced with niobium carbide obtained by polymer precursor, Mater. Res. 9 (2006) 271–274. https://doi.org/10.1590/S1516-14392006000300005.

[40] A. Nemamcha, H. Moumeni, J. L. Rehspringer, PVP Protective mechanism of palladium nanoparticles obtained by sonochemical process, Phys. Procedia 2 (2009) 713–717. https://doi.org/10.1016/j.phpro.2009.11.015.

[41] D. Ponnalagar, D. R. Hang, S. E. Islam, et al., Recent progress in two-dimensional Nb_2C MXene for applications in energy storage and conversion, Mater. Des. 231 (2023) 112046. https://doi.org/10.1016/j.matdes.2023.112046.

[42] Z. U. D. Babar, M. S. Anwar, M. Mumtaz, et al., Peculiar magnetic behaviour and Meissner effect in two-dimensional layered Nb_2C MXene, 2D Mater. 7 (2020) 035012. https://doi.org/10.1088/2053-1583/ab86d2.

[43] J. S. Zheng, B. Wang, A. L. Ding, et al., Synthesis of MXene/DNA/Pd/Pt nanocomposite for sensitive detection of dopamine, J. Electroanal. Chem. 816 (2018) 189–194. https://doi.org/10.1016/j.jelechem.2018.03.056.

[44] J. H. Yin, S. S. Pan, X. Guo, et al., Nb_2C MXene-functionalized scaffolds enables osteosarcoma phototherapy and angiogenesis/osteogenesis of bone defects, Nano-Micro. Lett. 13 (2021) 30. https://doi.org/10.1007/s40820-020-00547-6.

[45] T. T. Mao, F. Zhou, K. Han, et al., Self-standing reduced graphene oxide/Nb_2C MXene paper electrode with three-dimensional open structure for high-rate potassium ion storage, J. Phys. Chem. Solids 169 (2022) 110838. https://doi.org/10.1016/j.jpcs.2022.110838.

[46] R. D. K. Misra, Core-shell magnetic nanoparticle carrier for targeted drug delivery: challenges and design, Mater. Technol. 25 (2010) 118–126. https://doi.org/10.1179/175355510X12723642365241.

[47] H. Bagheri, N. Pajooheshpour, A. Afkhami, et al., Fabrication of a novel electrochemical sensing platform based on a core-shell nano-structured/molecularly imprinted polymer for sensitive and selective determination of ephedrine, RSC Adv. 6 (2016) 51135–51145. https://doi.org/10.1039/c6ra09488k.